Single-Crystal Epitaxial Thin Films of the Isotropic Metallic Oxides $Sr_{1-x}Ca_xRuO_3$ ($0 \leq x \leq 1$)

C. B. Eom,* R. J. Cava, R. M. Fleming, Julia M. Phillips,
R. B. van Dover, J. H. Marshall, J. W. P. Hsu, J. J. Krajewski,
W. F. Peck, Jr.

Single-crystal epitaxial thin films of the isotropic metallic oxides $Sr_{1-x}Ca_xRuO_3$ ($0 \leq x \leq 1$) were grown on miscut $SrTiO_3$(100) substrates in situ by 90° off-axis sputtering. These thin films exhibit low isotropic resistivities, excellent chemical and thermal stability, good surface smoothness, and high crystalline quality. Furthermore, the lattice parameters and magnetic properties can be varied by simply changing the strontium/calcium ratio. These epitaxial thin films, and their multilayer structures with other oxide materials, can be used for the fabrication of superconducting, ferroelectric, magneto-optic, and electro-optic devices.

Oxide materials exhibit a wide range of electrical properties: from superconducting, to metallic, to insulating. For device applications, it is necessary to have epitaxial growth of many of these types of oxide thin films in a single heterostructure. High-quality oxide thin films and multilayers have been successfully grown with superconducting and insulating properties (*1, 2*). In the present work, the growth and properties of high-quality, isotropic, metallic epitaxial thin films of $Sr_{1-x}Ca_xRuO_3$ are described.

In superconducting devices for use in integrated circuits, thin films of metallic oxides are required for superconductor–normal metal–superconductor (SNS) junctions and resistors. The resistivities of normal metals [such as Au, Ag (*3*), and Au-Ag alloys (*4*)] are very low; this low resistivity results in low I_cR products (critical current times junction resistance) in SNS junctions, leading to inferior device performance. Furthermore, one often needs to grow epitaxial superconducting thin films on top of the metal layers, and this is impossible with the materials listed above. Both layered perovskites (such as $PrBa_2Cu_3O_7$) (*5–7*) and isotropic perovskites (such as Nb-doped $SrTiO_3$) (*8*) have been used to make SNS junctions. However, the resistivity of $PrBa_2Cu_3O_7$ increases monotonically with decreasing temperature, and it is difficult to grow metallic Nb-doped $SrTiO_3$ thin films.

Ferroelectrics hold potential for both dynamic and permanent data storage in digital memory systems. At present, to build these memory devices, polycrystalline ferroelectric thin films are grown on a Pt or Al base electrode. The high-angle grain boundaries that occur in the ferroelectric thin film layer are detrimental to device performance because they cause aging and fatigue owing to charge segregation and decay at the grain boundaries. Ramesh *et al.* reported that thin film heterostructures of ferroelectric materials and certain cuprate superconductors have outstanding properties (*9*). These epitaxial device structures are attractive for nonvolatile memory applications because they lack detrimental high-angle grain boundaries in the ferroelectric layers and have coherent contacts between the electrodes and ferroelectric layers. Unfortunately, the cuprate superconductors are not fully chemically and thermally stable, which puts some constraints on their processing and usage. Furthermore, the high-T_c (superconducting transition temperature) superconducting cuprates typically have relatively poor crystalline quality and rough surfaces. These drawbacks may limit the application of such device structures for nonvolatile memory applications.

Recently, Lichtenberg *et al.* reported the epitaxial growth of $YBa_2Cu_3O_7$ thin films on metallic substrates of Sr_2RuO_4 single crystals (*10*). This substrate material is a paramagnetic conductor with the K_2NiF_4 structure. Because of its layered structure, Sr_2RuO_4 exhibits metallic behavior parallel to the layers but is semiconducting perpendicular to the layers. This anisotropic resistivity might be a problem for making devices.

In this report, we present results on $Sr_{1-x}Ca_xRuO_3$ epitaxial thin films. These films exhibit physical properties that may make them useful in some of these applications. These materials are pseudocubic perovskites (*11–13*) with essentially isotropic properties. Table 1 presents the space groups, lattice parameters, lattice distortions, and lattice mismatches of $Sr_{1-x}Ca_xRuO_3$ and $SrTiO_3$. The pseudocubic lattice parameters are the important factors when considering the lattice mismatches. The lattice mismatches are defined as $\epsilon_{a_o'}$ or $\epsilon_{c_o'} = [(a_o' \text{ or } c_o'/a_{o\ \text{substrate}}) - 1]$. The lattice distortions are indicated by the angle between [110] and [$\bar{1}$10] in the (001) plane. The lattice parameters can be tuned from 3.83 to 3.93 Å if the Sr/Ca ratio is varied, which allows us to grow epitaxial multilayers with many oxide materials that have an excellent lattice match on the (110) or (002) planes. Magnetic properties can also be varied from paramagnetic to ferromagnetic by varying the Sr/Ca ratio (*14*). The resistivity is low, less than 300 μohm-cm at room temperature (*14*). Furthermore, these ruthenates, unlike most oxide superconductors, are chemically and thermally very stable. In oxidizing or inert-gas atmospheres, $Sr_{1-x}Ca_xRuO_3$ is stable up to 1200 K (*15*).

We grew $SrRuO_3$, $CaRuO_3$, and $Sr_{0.5}Ca_{0.5}RuO_3$ films in situ by a 90° off-axis sputtering technique (*16, 17*). Substrate materials included miscut $SrTiO_3$(100), $LaAlO_3$(100), $NdGaO_3$(110), $NdGaO_3$(001), and MgO(100). The sputtering atmosphere consisted of 60 mtorr Ar and 40 mtorr O_2. The radio frequency power (125 W) on the $SrRuO_3$, $CaRuO_3$, and $Sr_{0.5}Ca_{0.5}RuO_3$ sputter guns generated a self-bias of −140, −220, and −200 V, respectively. The substrate block temperature was held at 680°C. These sputtering parameters gave a deposition rate of 0.2 Å s^{-1}. After deposition, the

Table 1. Space groups, lattice parameters, lattice distortions, and lattice mismatches of $Sr_{1-x}Ca_xRuO_3$ and $SrTiO_3$.

Materials	Space group	Lattice parameters (Å) (orthorhombic)	Lattice parameters (Å) (pseudocubic perovskite)	Lattice distortion	Lattice mismatch with $SrTiO_3$ (%)
$SrRuO_3$	*Pbnm* (no. 62)	$a_o = 5.53$	$a_o' = 3.93 = d_{(110)}$	89.6°	+0.64
	$GdFeO_3$ type	$b_o = 5.57$			
		$c_o = 7.85$	$c_o' = 3.93 = d_{(002)}$		
$Sr_{0.5}Ca_{0.5}RuO_3$	*Pbnm* (no. 62)	$a_o = 5.48$	$a_o' = 3.89 = d_{(110)}$	89.6°	−0.38
	$GdFeO_3$ type	$b_o = 5.52$			
		$c_o = 7.77$	$c_o' = 3.89 = d_{(002)}$		
$CaRuO_3$	*Pbnm* (no. 62)	$a_o = 5.36$	$a_o' = 3.85 = d_{(110)}$	88.2°	−1.41
	$GdFeO_3$ type	$b_o = 5.53$			
		$c_o = 7.66$	$c_o' = 3.83 = d_{(002)}$		−1.92
$SrTiO_3$			$a_o = b_o = c_o = 3.905$	90°	

AT&T Bell Laboratories, Murray Hill, NJ 07974.

*To whom correspondence should be addressed.

chamber was immediately vented in O_2 to a pressure of 300 torr, and the sample was then allowed to cool down. We deposited films with thicknesses from 500 to 2000 Å.

We measured the composition of 1000 Å thick $CaRuO_3$ and $SrRuO_3$ films on MgO(100) substrates with Rutherford backscattering spectroscopy (RBS). The film composition for $CaRuO_3$ was stoichiometric within experimental error. However, we could not directly measure the composition of $SrRuO_3$ because peaks from Sr (atomic number $Z = 38$) and Ru ($Z = 44$) cannot be resolved by 1.8-MeV $^4He^+$. By using a simulation program [RUMP (*18*)], we also found the $SrRuO_3$ films to be stoichiometric.

The film textures were investigated by x-ray diffraction with a four-circle diffractometer, a Cu K_α source, and a pyrolytic graphite monochromator and analyzer. The films were aligned so that the film normal was parallel to the ϕ axis of the diffractometer. This geometry allows full access to the reciprocal lattice (except for in-plane reflections) with $\omega = \phi$. Figure 1A shows the θ-2θ scans of $SrRuO_3$ and $CaRuO_3$ thin films grown on $SrTiO_3$(100) substrates. The only substantial peaks detected are from *d* spacings (interatomic distances) corresponding to (110) or (002). Because of the systematic absence of a (00ℓ) peak ($\ell = 2n - 1$) and the near-degeneracy of $d_{(110)}$ and $d_{(002)}$ in the pseudocubic $SrRuO_3$ and $CaRuO_3$ structures, it was not possible to distinguish from the normal θ-2θ scans alone whether the texture is (110) or (002) or a combination. We were able to establish that these films are purely (110) texture normal to the substrate by locating peaks that do not have a degenerate pair, such as the (113) peak. This peak was observed only at the position corresponding to (110) grains normal to the substrate and was not observed at the position corresponding to (002) grains. Peaks with degenerate pairs cannot be used to distinguish the texture; for example, (121) peak positions for (110) grains normal to the substrate are the same as those of the (103) peak positions for (002) grains normal to the substrate. After we established pure (110) film texture, we could assign unique indexes to pairs of peaks with near-degenerate *d* spacing and study in-plane texture. In a similar scan for a $Sr_{0.5}Ca_{0.5}RuO_3$ film grown on a $SrTiO_3$(100) substrate, we were not able to resolve film peaks because the strong substrate peaks overlap them. However, we were able to find (110) film peaks on $LaAlO_3$(100) and $NdGaO_3$(110) substrates as a result of the different lattice parameters.

We also investigated the in-plane textures for these films by scanning off-axis peaks. Figure 1B shows ω scans of the (221) reflection at ϕ = 0°, 45°, 90°, 180°, and 270° for a (110) $SrRuO_3$ thin film on $SrTiO_3$(100). [We observed the same results with the nondegenerate (113) reflection.] The significant intensities only at ϕ = 0° and 180°, but zero intensity at ϕ = 45°, 90°, and 270°, clearly indicate that the grains are single domain with in-plane epitaxial arrangement of $SrRuO_3[\bar{1}10]//SrTiO_3[010]$ and $SrRuO_3[001]//SrTiO_3[001]$. The intensity ratio $I(\phi = 0°)/I(\phi = 90°) > 10^3$ indicates that the volume fraction of the second variant grains is less than 0.1%. The $SrTiO_3$(100) substrate was found to be miscut 2.3°, and the projection of the surface normal is 20° away from the in-plane $SrRuO_3$ 44[001] direction. We believe that the miscut substrate must be responsible for promoting single domain growth as observed in (103) oriented $La_{2-x}Sr_xCuO_4$ (*19*) and $Bi_2Sr_2CaCu_2O_8$ (*20, 21*) thin films. In contrast, $CaRuO_3$ thin films showed significant intensities at both ϕ = 0° and 90°, in spite of the similarly miscut $SrTiO_3$(100) substrate, which indicates the presence of two types of domains with approximately equal populations, and in-plane epitaxial arrangements of $CaRuO_3[001]$, $[\bar{1}10]//SrTiO_3[001]$, and $CaRuO_3[001]$, $[\bar{1}10]//SrTiO_3[010]$.

The x-ray data reveal a lattice parameter expansion along the growth direction in $SrRuO_3$ thin films. The lattice parameter ($d_{(110)}$) is 3.96 Å, whereas that of the bulk ($d_{o\ (110)}$) is 3.93 Å. When a thin film is subject to compressive strain (ϵ_{xx} or ϵ_{yy}) in the plane, the result is tensile strain perpendicular to the substrate (ϵ_{zz}). The strain can be calculated from the above lattice parameters:

$$\epsilon_{zz} = \frac{d_{(110)} - d_{o\ (110)}}{d_{o\ (110)}} = \frac{3.96\ \text{Å} - 3.93\ \text{Å}}{3.93\ \text{Å}} = 0.0076 \qquad (1)$$

If we assume that the film is elastically isotropic and Poisson's ratio $\nu \approx 0.3$, the compressive biaxial strain in the film can be calculated by the formula

$$\epsilon_{xx} = \epsilon_{yy} = -\frac{1-\nu}{2\nu}\epsilon_{zz} = 0.0089 \qquad (2)$$

Then, we can estimate the two in-plane pseudocubic lattice parameters $d_{(\bar{1}10)} = d_{(001)} = 3.90$ Å. Although the measured in-plane lattice parameters from (220),

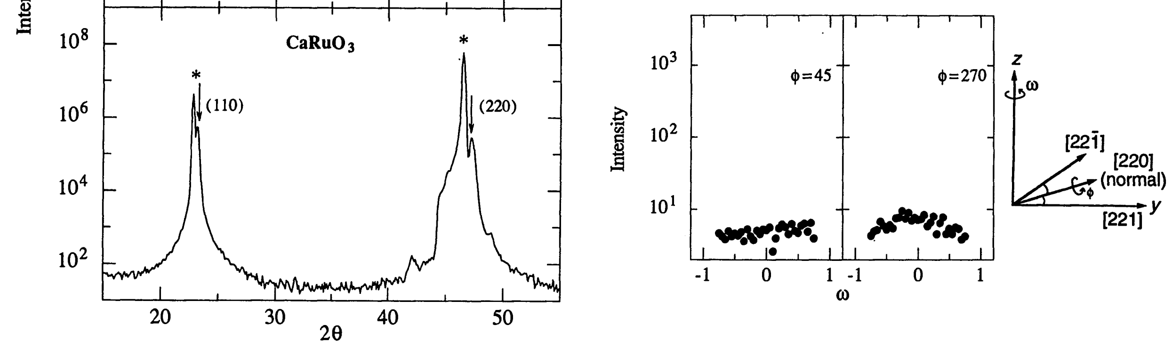

Fig. 1. (**A**) X-ray diffraction θ-2θ scans of $SrRuO_3$ and $CaRuO_3$ thin films on $SrTiO_3$(100) substrates. The $SrTiO_3$ peaks are marked (*). (**B**) X-ray ω scans of the (221) reflection at ϕ = 0°, 45°, 90°, 180°, and 270° for a (110)-oriented $SrRuO_3$ thin film on a $SrTiO_3$(100) substrate showing a single variant domain. The inset shows the diffraction geometry. The diffraction condition is met when the reciprocal lattice direction is parallel to the $\hat{y}$ axis.

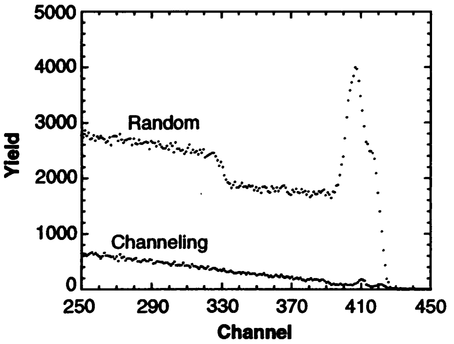

Fig. 2. Rutherford backscattering spectrum showing energy versus intensity for both channeling and random 1.8-MeV $^4He^+$ ions backscattered from a $SrRuO_3$ thin film on a $SrTiO_3(100)$ substrate; χ_{min} is 1.8%, which is very close to the value of a Si single crystal.

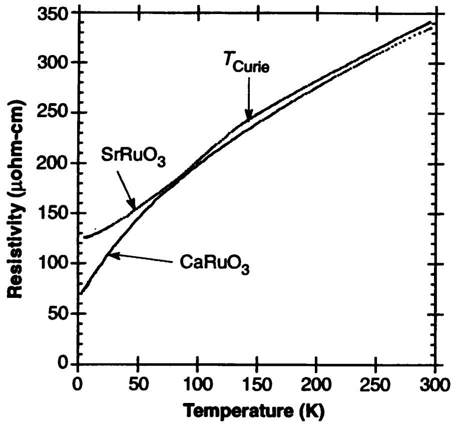

Fig. 4. Resistivity versus temperature curves for $SrRuO_3$ and $CaRuO_3$ thin films 1000 Å thick on $SrTiO_3(100)$ substrates; T_{Curie} is the Curie temperature for the paramagnetic-ferromagnetic transition in $SrRuO_3$.

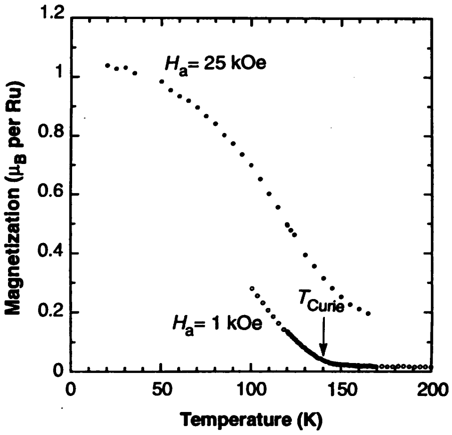

Fig. 5. Magnetization per formula unit versus temperature curves for a $SrRuO_3$ thin film 1000 Å thick on a $SrTiO_3(100)$ substrate, measured at fields, H_a, of 1 and 25 kOe in a SQUID magnetometer.

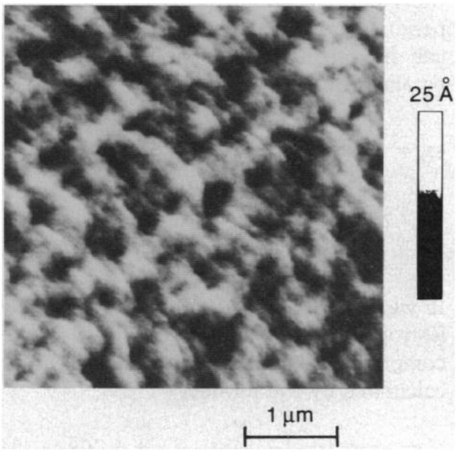

Fig. 3. Surface morphology of a $SrRuO_3$ thin film 2000 Å thick on a $SrTiO_3(100)$ substrate imaged with an atomic force microscope. The gray scale of the picture from white to black is 25 Å and the area is 4 μm by 4 μm.

(113), (121), (111), (221), and (223) type reflections, which give $d_{(001)}$ = 3.90 Å, are not as accurate as that of $d_{(110)}$, they are consistent with the above arguments. This lattice parameter is very similar to the $SrTiO_3$ substrate lattice parameter (3.905 Å), suggesting that the film-substrate interface is coherent. However, the lattice parameters of $CaRuO_3$ films are the same as those of single crystals and bulk samples (*13*). In the case of $CaRuO_3$ thin films, the lattice mismatch with $SrTiO_3$ substrates is large, and there is less persistence of structural coherency at the interface during film growth. This is consistent with the crystalline quality of those films studied by rocking curve width.

The ω scan rocking curve widths (full width at half maximum) of the (220) reflections of $SrRuO_3$ and $CaRuO_3$ are 0.16° and 0.58°, respectively. These measurements are limited by the instrument resolution of 0.16°. The better crystalline quality of $SrRuO_3$ as compared to $CaRuO_3$ is probably the result of its better lattice match with the $SrTiO_3(100)$ substrate and smaller orthorhombic distortion (*14*). On the basis of this explanation, we believe that the best crystalline quality $CaRuO_3$ thin films can be grown on $CaTiO_3$ substrates.

We investigated the crystalline quality of the films by ion channeling. Figure 2 shows the aligned <100> and random RBS spectra (1.8 MeV $^4He^+$ ions) for a $SrRuO_3$ film on $SrTiO_3(100)$. The ratios (χ_{min}) of the backscattered yield for a $SrRuO_3$ and a $Sr_{0.5}Ca_{0.5}RuO_3$ film along <100> to that in a random direction are 1.8 and 2.1%, respectively, which are very close to the value of Si single crystals. However, a $CaRuO_3$ thin film on $SrTiO_3$ has χ_{min} of 50%, which is consistent with the x-ray rocking curve data.

A smooth surface is very important for the fabrication of devices with multilayer structures. We investigated the surface morphology of these films by scanning electron microscopy (SEM). The surface of $SrRuO_3$ and $CaRuO_3$ films 2000 Å thick was found to be featureless with a lateral resolution of 100 Å. The films were further examined with an atomic force microscope (AFM) [Parks Scientific Instrument model SFM-BD2, with Ultralevers] (tip radius ~ 100 Å). Figure 3 shows an AFM image on a $SrRuO_3$ thin film 2000 Å thick on $SrTiO_3(100)$ over a 4 μm by 4 μm area. Results from five scans of the same size but over different spots on the same film revealed a root mean square surface roughness of 6.9 ± 0.2 Å and a peak-to-valley roughness of 53 ± 6 Å. To the best of our knowledge, this is the smoothest surface of any perovskite thin film ever reported. As seen in Fig. 3, no screw dislocations were observed, in contrast to the case for $YBa_2Cu_3O_7$ thin films grown by the same process (*22, 23*). We have occasionally observed protrusions of <200 Å in height and ~2000 Å lateral dimensions. Comparable density and dimensions of protrusions were also seen on the $SrTiO_3$ substrate (*24*) with an AFM. Therefore, these protrusions are probably due to substrate defects that cause growth rates to be inhomogeneous. We believe that the growth of $SrRuO_3$ films on $SrTiO_3$ occurs layer by layer, resulting in very smooth surfaces. This conclusion is consistent with the x-ray data showing the films to be single domain.

We measured normal state resistivities of the thin films as a function of temperature by the four-terminal transport method. Film thicknesses were measured by profilometry at film edges made by selective deposition through Si shadow masks and compared with results from RBS measurements. The results from the two measurements were consistent to within 10%. Figure 4 shows resistivity versus temperature curves for $SrRuO_3$ and $CaRuO_3$ films 1000 Å thick on $SrTiO_3(100)$. The resistivity behavior along the two orthogonal directions is the same, which is expected because these are isotropic materials. The resistivity at room temperature (ρ_{300}) is ~340 μohm-cm, and the temperature dependences ($d\rho/dT$) show good metallic behavior. These normal-state resistivities are slightly higher than those reported for high-quality single crystals; these differences might be due to strain in the film or uncertainty in the film thickness. The temperature at which a pronounced break occurs in the curve for $SrRuO_3$ agrees with the reported Curie temperature, T_{Curie} (150 K). The resistivity at room temperature for $Sr_{0.5}Ca_{0.5}RuO_3$ film is comparable to those of $CaRuO_3$ and $SrRuO_3$ films.

We measured the magnetization at fields of 1 and 25 kOe in a SQUID (superconducting quantum interference device) magnetometer, as a function of temperature for a $SrRuO_3$ film of thickness 1000 Å (Fig. 5). The magnetization is reported in units of Bohr magnetons (μ_B) per Ru atom. The saturation moment is roughly 1.05 μ_B, a value that is consistent with the literature. The ferromagnetic transition is significantly broadened in such a high field; low-field measurements indicate a T_{Curie} of about 140 K, slightly lower than that reported for bulk (*25*) and single-crystal (*14*) material, 150 to 160 K. The large field is required to obtain saturation owing to the large anisotropy energy, $\sim 10^6$ to 10^7 erg/cm^3, reported for this material. It has been reported that $CaRuO_3$ orders antiferromagnetically with a T_{Curie} of ~110 K (*14*), but we were unable to resolve any transition in our films. This result is consistent with the lack of any inflection in the resistivity curve and may indicate the absence of long-range order. This result is also consistent with the Mossbauer data (*26*), which give no evidence for antiferromagnetic ordering in $CaRuO_3$. The unique magnetic properties of these thin films offer new opportunities for studying superconductivity through model experiments.

We have already prepared epitaxial heterostructures with high-T_c superconductors ($YBa_2Cu_3O_7/Sr_{1-x}Ca_xRuO_3$) (*27*). These heterostructures are structurally and electrically as good as the individual single-layer thin films on $SrTiO_3(100)$ substrates. We have also fabricated epitaxial ferroelectric heterostructures with a ferroelectric material [$SrRuO_3/Pb(Zr_{0.52}Ti_{0.48})O_3/SrRuO_3$]. These heterostructures have a high crystalline quality and clean interfaces as revealed by x-ray diffraction, RBS, and cross-sectional transmission electron microscopy. The ferroelectric layers exhibit superior fatigue and retention characteristics over 10^{10} cycles at 20 kHz and 10 V with a large remnant polarization (27 μC/cm^2) (*27*). These multilayer structures can be used for the fabrication of superconducting, ferroelectric, magneto-optic, and electro-optic devices (*27*).

REFERENCES AND NOTES

1. J.-M. Triscone *et al.*, *Phys. Rev. Lett.* **64**, 804 (1990).
2. C. B. Eom *et al.*, *Science* **251**, 780 (1991).
3. M. S. Dilorio, S. Yoshizumi, K.-Y. Yang, J. Zhang, M. Maung, *Appl. Phys. Lett.* **58**, 2552 (1991).
4. R. H. Ono *et al.*, *ibid.* **59**, 1126 (1991).
5. C. T. Rogers *et al.*, *ibid.* **55**, 2032 (1988).
6. J. Gao *et al.*, *IEEE Trans. Magn.* **27**, 3062 (1991).
7. T. Hashimoto, M. Sagoi, Y. Mizutani, J. Yoshida, K. Mizushima, *Appl. Phys. Lett.* **60**, 1756 (1992).
8. D. K. Chin and T. Van Duzer, *ibid.* **58**, 753 (1991).
9. R. Ramesh *et al.*, *Science* **252**, 944 (1991).
10. F. Lichtenberg, A. Catana, J. Mannhart, D. G. Schlom, *Appl. Phys. Lett.* **60**, 1138 (1992).
11. J. Randall and R. Ward, *J. Am. Chem. Soc.* **81**, 2629 (1959).
12. A. Callaghan, C. W. Moeller, R. Ward, *Inorg. Chem.* **5**, 1572 (1966).
13. P. R. Van Loan, *Ceram. Bull.* **51**, 231 (1972).
14. R. J. Bouchard and J. L. Gillson, *Mater. Res. Bull.* **7**, 873 (1972).
15. W. Bensch, H. W. Schmalle, A. Reller, *Solid State Ionics* **43**, 171 (1990).
16. C. B. Eom *et al.*, *Appl. Phys. Lett.* **55**, 595 (1989).
17. C. B. Eom *et al.*, *Physica C* **171**, 351 (1990).
18. L. R. Doolittle, *Nucl. Instrum. Methods B* **9**, 344 (1985).
19. J. Kwo, R. M. Fleming, H. L. Kao, D. J. Werder, C. H. Chen, *Appl. Phys. Lett.* **60**, 1905 (1992).
20. Osamu Wada *et al.*, *Jpn. J. Appl. Phys.* **30**, L722 (1991).
21. Osamu Wada *et al.*, *ibid.*, p. L1881.
22. M. Hawley *et al.*, *Science* **251**, 1587 (1991).
23. C. Gerber, D. Anselmetti, J. G. Bednorz, J. Mannhart, D. G. Schlom, *Nature* **350**, 279 (1991).
24. Commercial Crystal Laboratories, Inc., Naples, FL (unpublished data).
25. Akio Kanbayashi, *J. Phys. Soc. Jpn.* **44**, 108 (1978).
26. T. C. Gibb *et al.*, *J. Chem. Soc. Dalton Trans.* **1973**, 1253 (1973).
27. C. B. Eom *et al.*, in preparation.
28. We thank D. W. Murphy and A. F. Hebard for helpful discussions.

4 August 1992; accepted 9 October 1992

Open Framework Structures Based on Se_x^{2-} Fragments: Synthesis of $(Ph_4P)[M(Se_6)_2]$ (M = Ga, In, Tl) in Molten $(Ph_4P)_2Se_x$

Sandeep Dhingra and Mercouri G. Kanatzidis*

Polychalcogenide compounds with open polymeric frameworks are rare, and they represent a class of compounds in which microporosity might be achieved. Microporous frameworks that are not oxide-based are now attracting interest because of the combination of catalytic and electronic properties they may simultaneously possess. Three new compounds that may be forerunners to such materials have been discovered and are reported here. The reaction of gallium (Ga), indium (In), and thallium (Tl) metal with $(Ph_4P)_2Se_5$ (Ph, phenyl) and an excess of elemental selenium (Se) in a sealed, evacuated Pyrex tube at 200°C yielded small red crystals of $(Ph_4P)[Ga(Se_6)_2]$ (I), $(Ph_4P)[In(Se_6)_2]$ (II), and $(Ph_4P)[Tl(Se_6)_2]$ (III), respectively. The $[M(Se_6)_2]^-$ (M = Ga, In, Tl) ions form a two-dimensional, open framework filled with Ph_4P^+ ions. The $[M(Se_6)_2]_n^{n-}$ structure consists of tetrahedral M^{3+} centers and bridging Se_6^{2-} ligands, leading to an extended structure in two dimensions. These layers stack perfectly one on top of the other giving rise to one-dimensional channels running down the *c* axis that are filled with Ph_4P^+ cations. These cations are situated in the layers, as opposed to between the layers, and the whole structure can be viewed as a template. Compound II shows remarkable thermal stability and melts congruently at 242°C. Upon cooling to room temperature it gives a glassy phase that recrystallizes upon subsequent heating to 160°C.

There is an increasing interest in new and unusual synthetic conditions that may help stabilize new compounds with novel structural frameworks and interesting physical properties that are not possible by conventional techniques. Soluble and solid-state metal chalcogenides are undergoing intense investigation owing to their interesting electrical (*1, 2*), optical (*3, 4*), and catalytic properties (*5*), as well as their unusual structural features (*6–23*). Conventionally, syntheses of molecular metal polychalcogenides take place in solution at ambient temperature (*6–12*), whereas syntheses of solid-state metal chalcogenides are performed at temperatures higher than 500°C (*13–16*). In the past few years, fluxes of molten alkali metal polychalcogenides (*17–20*) have been used as reaction media to synthesize novel solid-state materials in the relatively low-temperature regime of 150° to 500°C. Recently, we have shown that the hydrothermal technique represents another direction for the synthesis of some exotic materials made of metal polychalcogenides (*21–23*). Given the enormous utility of microporous oxides (such as zeolites) in chemical technology and the corresponding prominence of metal chalcogenides in electronic applications, it is worthwhile to envision materials that combine the useful properties of both into one new class of microporous chalcogenides. Although such materials have not been reported to exist, a few publications have made reference to this concept (*24, 25*). To extend this work and obtain solids with large organic cations in their lattice, we undertook a synthetic approach using the reactive $(Ph_4P)_2Se_x$ in molten form as a reaction media to incorporate the organic cations as templates in order to stabilize open, anionic, metal-polyselenide frameworks. Herein we report the synthesis, structural characterization, and thermal properties of three isostructural compounds, $(Ph_4P)[Ga(Se_6)_2]$ (I), $(Ph_4P)[In(Se_6)_2]$ (II),

---

Department of Chemistry and Center for Fundamental Materials Research, Michigan State University, East Lansing, MI 48824.

*To whom correspondence should be addressed.